


Host defense functions of the epididymal amyloid matrix

Caitlyn Myers¹, Mary Catherine Hastert², and Gail A. Cornwall ^{1,*}

¹Department of Cell Biology and Biochemistry, Texas Tech University Health Sciences Center, Lubbock, TX, USA ²College of Arts and Sciences Microscopy, Texas Tech University, Lubbock, TX, USA

*Correspondence address. Department of Cell Biology and Biochemistry, Texas Tech University Health Sciences Center, Lubbock, TX 79430, USA; E-mail: gail.cornwall@ttuhsc.edu  <https://orcid.org/0000-0002-2903-1690>

Submitted on August 5, 2022; resubmitted on October 17, 2022; editorial decision on November 8, 2022

ABSTRACT: The epididymal lumen is an immunologically distinct environment. It maintains tolerance for the naturally antigenic spermatozoa to allow their maturation into functional cells while simultaneously defending against pathogens that can ascend the male tract and cause infertility. We previously demonstrated that a nonpathological amyloid matrix that includes several cystatin-related epididymal spermatogenic (CRES) subgroup family members is distributed throughout the mouse epididymal lumen but its function was unknown. Here, we reveal a role for the epididymal amyloid matrix in host defense and demonstrate that the CRES amyloids and CD-1 mouse epididymal amyloid matrix exhibit potent antimicrobial activity against bacterial strains that commonly cause epididymal infections in men. We show the CRES and epididymal amyloids use several defense mechanisms including bacterial trapping, disruption of bacterial membranes and promotion of unique bacterial ghost-like structures. Remarkably, these antimicrobial actions varied depending on the bacterial strain indicating CRES amyloids and the epididymal amyloids elicit strain-specific host defense responses. We also demonstrate that the CRES monomer and immature assemblies of the epididymal amyloid transitioned into advanced structures in the presence of bacteria, suggesting their amyloid-forming/shape-shifting properties allows for a rapid reaction to a pathogen and provides an inherent plasticity in their host defense response. Together, our studies reveal new mechanistic insight into how the male reproductive tract defends against pathogens. Future studies using a mouse model for human epididymitis are needed to establish the epididymal amyloid responses to pathogens *in vivo*. Broadly, our studies provide an example of why nature has maintained the amyloid fold throughout evolution.

Key words: amyloid / epididymis / reproductive tract / host defense / cystatin / CRES / bacterial ghost / *E. coli* / epididymitis

Introduction

The epididymis is a highly convoluted tubule through which spermatozoa must pass after leaving the testis to acquire their functions of progressive motility and the ability to fertilize an oocyte. Since spermatozoa are synthetically inactive, their maturation process requires interacting with proteins and other molecules secreted into the lumen by the surrounding epididymal epithelium. In addition to maturation, the epididymis must also protect the spermatozoa, and the developing germ cells in the testis, from pathogens that can ascend the male tract and cause transient or permanent infertility. Because spermatogenesis occurs after self-tolerance has been established, spermatozoa are naturally antigenic (Wheeler *et al.*, 2011; Tung *et al.*, 2017). Therefore, the epididymal lumen is an immunologically distinct compartment that maintains a tolerant environment for spermatozoa to mature into functional cells. The epididymal lumen must also have the ability to mount a robust host defense response against pathogens that might access the male tract. Toward this end, the epididymis relies heavily on the innate immune system and its antimicrobial

peptides (AMPs) and proteins for host defense. For example, the rodent and human epididymal epithelium secretes multiple β -defensins, SPAG11 (HE2) and its isoforms, cathelicidin (hCAP18, mouse CAMP) and other AMPs into the lumen (Malm *et al.*, 2000; Yenugu *et al.*, 2003; Hall *et al.*, 2007; Yenugu and Narmadha, 2010). The epididymis also secretes several antimicrobial proteins including the secretory leukoprotease inhibitor (SLPI), lactoferrin, lysozyme, epididymal protease inhibitor (EPPIN), lipocalin-2 and others (Jin *et al.*, 1997; Hall *et al.*, 2002; Yenugu *et al.*, 2004; Jenssen and Hancock, 2009; Silva *et al.*, 2012). Despite their critical roles in protecting the germline, mechanisms by which the epididymal AMPs and proteins defend against pathogens remain poorly understood.

We previously demonstrated that a constitutively produced, nonpathological amyloid matrix is present throughout the normal mouse epididymal lumen (Whelley *et al.*, 2012, 2016). Its functional role in the epididymis has not been established. Highly ordered cross- β -sheet-rich amyloids have typically been considered as pathological entities associated with neurodegenerative diseases and prionopathies. Work from our laboratory and others have shown, however, that functional

amyloid assemblies exist in species ranging from bacteria to humans. These biological amyloids carry out a broad range of functions including acting as biological scaffolds, storage depots, protective barriers and signaling complexes (Fowler et al., 2007; Pham et al., 2014; Hewetson et al., 2017) (reviews). The epididymal amyloid matrix includes several members of the reproductive cystatin-related epididymal spermatogenic (CRES) subgroup of family 2 cystatins of cysteine protease inhibitors. CRES subgroup members CRES (Cst8), CRES2 (Cst11), CRES3 (Cst12), cystatin E2 and the ubiquitously expressed, prototypical family 2 cystatin, cystatin C (Cst3), colocalize within the epididymal amyloid matrix, suggesting coordinated functions (Whelley et al., 2016). In addition, CRES has lost its cysteine protease inhibitory activity, but subgroup members maintain robust amyloidogenic/shape-shifting functions (Cornwall et al., 2003; Whelley et al., 2016). CRES and CRES2 are expressed in the human epididymis but whether they assemble into a functional amyloid has not been determined (Hamil et al., 2002; Wassler et al., 2002). Recombinant cystatin C (human) and CRES subgroup members CRES (mouse), CRES2 (human) and testatin (Cst9, human) have also been shown to exhibit antimicrobial activity *in vitro* and may represent a new family of antimicrobial proteins (Hamil et al., 2002; Wang et al., 2012; Eaves-Pyles et al., 2013; Holloway et al., 2018). Whether their antimicrobial activities require an amyloid structure is not known.

Here, we present results showing a biological role for the mouse epididymal amyloid matrix in host defense. CRES amyloids and the epididymal amyloid matrix use multiple mechanisms, including bacterial trapping and membrane disruption, to protect against pathogens that commonly cause human epididymal infections. In addition to these classic responses, CRES amyloid and the epididymal amyloids also promoted the formation of unique bacterial ghost-like structures, not previously described in the epididymis or known to be in response to amyloid. We also show that CRES monomer and immature epididymal amyloid formed advanced amyloid structures in the presence of bacteria to enable their antimicrobial actions, a response similar to other host defense amyloids. However, CRES and the epididymal amyloid matrix are distinct as they formed different amyloid structures and elicited different host defense responses (trapping versus killing) depending upon the pathogen. Together our studies show the epididymal amyloid matrix is a multidimensional antimicrobial amyloid that uses its unique shape-shifting properties to protect the host via several mechanisms.

Materials and methods

Isolation of epididymal amyloids

All animal studies were conducted in accordance with the NIH Guidelines for the Care and Use of Experimental Animals using protocol # 94041 approved by the Texas Tech University Health Sciences Center Institutional Animal Care and Use Committee. Male CDI mice (22–28 weeks of age) were obtained from Charles River (Wilmington, MA, USA) and maintained under a constant 12 h light/12 h dark cycle with food and water *ad libitum*. Nestlets were provided for nesting. Two mice were used for each experiment and were euthanized by CO₂ asphyxiation followed by cervical dislocation. The luminal contents from the caput and corpus-cauda epididymis were isolated by

puncturing the tissue in Dulbecco's PBS (dPBS) using a 30G needle and allowing material to disperse for 15 min at room temperature. The samples were centrifuged at 500g for 5 min to remove spermatozoa (pellet 1: P1). The S1 supernatant was spun again to remove any remaining spermatozoa and then centrifuged at 5000g for 10 min to generate pellet 2 (P2). The resulting supernatant (S2) was centrifuged at 15 000g for 10 min to generate pellet 3 (P3) followed by centrifugation of the S3 supernatant at 250 000g for 70 min using a table-top Beckman ultracentrifuge to generate the final S4 supernatant (SUP) and P4 pellet (P4). All pellets were resuspended in dPBS and proteins quantified by BCA assay (ThermoScientific, Rockford, IL, USA).

Expression, purification and assembly of CRES^{C48A} protein into amyloid

Tag-less full-length mouse CRES^{C48A} protein was expressed and purified as described previously using affinity, ion exchange and gel filtration chromatography (Do et al., 2019). Immediately after elution off the gel filtration column, CRES^{C48A} was buffer exchanged into 25 mM MES, pH 6 using a 10 kDa Amicon-Ultra-15 filter (Millipore, Burlington, MA, USA). Briefly, ~2.5 mg of protein in 20–30 ml was combined and spun in a 10-kDa Amicon-Ultra filter (14 ml at a time) (Millipore) at 2550g, 4°C, in a swinging bucket rotor until 1 ml of protein remained. The protein was moved to a new 10 kDa Amicon-Ultra-15 filter and 13 ml of 25 mM MES, pH 6.0, was added. The protein was spun at 2550g until 1 ml remained. Another 13 ml of 25 mM MES, pH 6.0, was added to the protein in the filter unit, the sample gently mixed by pipetting and 1 ml removed as the CRES^{C48A} monomer (0.14–0.19 mg/ml concentration). The remaining protein was centrifuged at 2550g until 1 ml remained (~2 mg/ml final concentration). The protein was moved to a 1.5 ml microcentrifuge tube and 250 µl was removed as 'Early Amyloid'. Then, 250 µl 50 mM HEPES, pH 8.0, was added to the ~750 µl of remaining protein (the amount of 50 mM HEPES, pH 8, added is 1/4 the final volume) and the sample was spun in a 10 kDa Amicon-Ultra filter (0.5 ml) at 16 100g, 4°C in a microcentrifuge until 100 µl remained. The filter was inverted in a new tube and spun at 1000g for 2 min to elute protein off the filter. An aliquot (50 µl) was removed as 'Intermediate Amyloid' and typically was ~12–14 mg/ml, pH 6.8. Monomer, Early Amyloid, Intermediate Amyloid and remaining protein (~40–50 µl) were kept at 4°C overnight. The next morning, the remaining protein was sonicated at 3 × 30 pulses at 20% duty, 1 × 30 pulses at 30% duty and 1 × 30 pulses at 50% duty using a Heat Systems Ultrasonic sonicator (Qsonica, Newtown, CT, USA) and the resulting suspension (~12–14 mg/ml) was the 'Advanced Amyloid'. Protein concentrations were determined using a Nanodrop Lite spectrophotometer (ThermoScientific, Rockford, IL, USA). The CRES^{C48A} monomer and different amyloid preparations were used immediately.

Colony-forming unit assay

The pathogenic *Escherichia coli* strain UI012 was a generous gift from Abdul Hamood, Ph.D., Texas Tech University Health Sciences Center, who obtained the clinical isolate under an Institutional Review Board approved protocol. The commensal *E. coli* strain MM294 was also a gift from A. Hamood and obtained from the American Type Culture Collection (Manassas, VA, USA). *E. coli* were grown overnight (16 hr) in Luria–Bertani (LB) broth at 37°C with shaking at 180 rpm.

The overnight culture was used to start a log phase growth and bacteria were grown for 2 hr to OD_{600} 0.5. One milliliter of the log phase bacteria was centrifuged at 9000g for 5 min and resuspended in 1 ml dPBS, pH 6.8 (Sigma Chemical Co, St. Louis, MO, USA) to wash bacteria free of LB. The spin was repeated twice and the final pellet was resuspended in dPBS to an OD_{600} 0.5 ± 0.03 . Bacteria were serially diluted 1:10 in dPBS, pH 6.8 and 20 μ l 10^{-3} bacteria were added to 20 μ l CRES^{C48A} monomer and amyloids (final concentration 0.5–20 μ g/ml) and 85 μ l dPBS, pH 6.8 (assay buffer, final volume 125 μ l) in a low protein binding 96-well plate (Costar 7007, Corning, Coming, NY, USA). Incubations were carried out for 2 hr at 37°C with shaking at 150 rpm. The reactions were diluted 1:10 in dPBS, pH 6.8, and 25 μ l plated onto LB agar plates for overnight growth at 37°C. The number of colony-forming units (CFUs) was determined by manual counting of colonies. The percentage survival was calculated by comparing the CFUs in the presence of protein/CFUs in control (bacteria incubated in buffer only). The number of bacterial CFUs used in each assay was determined by plating 10^{-5} to 10^{-6} dilutions of each bacterial culture on LB agar plates followed by manual counting of colonies the next day. The average number \pm SEM of bacterial CFUs for *E. coli* MM294 was 4833 ± 806 and *E. coli* UI012, 2343 ± 156 . The same protocol was used for CFU assays with the epididymal amyloids except that 25 mM HEPES, pH 6.8 was used in place of dPBS throughout the assay. The average number \pm SEM of bacterial CFUs for *E. coli* MM294 was 2895 ± 708 , and *E. coli* UI012, 1418 ± 85 .

Live-dead assay

Bacterial strains were prepared as described in the CFU assay. Twenty microliters of 10^{-2} bacteria were incubated with 20 μ l of 5–30 μ g/ml protein and 85 μ l of 25 mM HEPES, pH 6.8 (assay buffer) in a low protein binding 96-well plate. Five microliters of 500 μ g/ml DAPI (20 μ g/ml final) and 5 μ l 125 μ g/ml propidium iodide (PI: 5 μ g/ml final) were added to the samples and incubated at room temperature in the dark for 20 min. The samples were centrifuged at 12 200g in a swinging bucket rotor for 45 min and the majority of the supernatant removed. The remaining \sim 10 μ l was used to resuspend the bacteria and 4 μ l were spotted on to a slide, a coverslip added, and images immediately captured using a Zeiss Axiovert 200M microscope equipped with epifluorescence (Zeiss, Okerkochen, Germany). The percentage of bacteria with intact membranes was calculated by the number of healthy bacteria/the total number of bacteria counted \times 100. Ghosts were not included in the percentages calculated for bacteria with intact membranes.

Negative stain transmission electron microscopy

Twenty microliters of 10^{-2} bacteria were incubated with 20 μ l of 20 μ g/ml protein and 85 μ l of dPBS, pH 6.8, or 25 mM HEPES, pH 6.8 (assay buffer) in a low protein binding 96-well plate (Costar, Kennebunk, ME, USA). Incubations were carried out for 2 hr at 37°C with shaking at 150 rpm. The samples were centrifuged twice at 12 200g in a swinging bucket for 15 min and majority of the supernatant was removed. For transmission electron microscopy (TEM), 5 μ l of the reactions were spotted on to Formvar/carbon-coated

200 mesh nickel grids (Ted Pella, Redding, CA, USA) and allowed to dry. The sample was washed for 1 min with water, stained with 1% uranyl acetate for 1 min, washed twice with water for 1 min and dried for 2 min. Grids were examined with a Hitachi 7650 electron microscope (Hitachi High-Tech America, Schaumburg, IL, USA).

Bacterial trapping/immunofluorescence

E. coli strain MM294 was grown overnight (16 hr) in LB at 37°C with shaking at 180 rpm. The overnight culture was used to start a log phase growth and bacteria were grown for 2 hr to OD_{600} 0.5. One milliliter of the log phase bacteria was centrifuged at 9000g for 5 min and resuspended in 150 μ l of 20 μ g/ml of DAPI. Bacteria were incubated at room temperature in the dark for 20 min. Then, bacteria were spun at 9000g for 5 min, resuspended in 1 ml dPBS to remove remaining DAPI, spun again and resuspended in dPBS to OD_{600} 0.5 ± 0.03 . Twenty microliters of 10^{-1} bacteria were incubated with 20 μ l of 20 μ g/ml (final) protein and 85 μ l of 25 mM HEPES (assay buffer) in a low protein binding 96-well plate. Incubations were carried out for 15 min at 37°C with shaking at 150 rpm. Samples were fixed for 15 min by adding formaldehyde (4% final) to each well. Samples were spun at 12 200g in a swinging bucket rotor for 15 min and the majority of the supernatant was removed. The bacteria were resuspended in the remaining volume (\sim 10 μ l) and 5 μ l of each reaction was spread on a slide (\sim 1 cm \times 1 cm square) and dried overnight. Slides were rehydrated in dPBS for 2 min and then blocked in 100% heat-inactivated goat serum (HIGS) (Vector Laboratories, Newark, CA, USA) for 1 hr at room temperature followed by incubation with rabbit anti-oligomeric amyloid A11 antiserum (1:1500) (Millipore, Billerica, MA, USA), rabbit anti-fibrillar amyloid OC antiserum (1:1500) (Millipore), or normal rabbit serum (1:1500) (ThermoScientific) in 20% HIGS/dPBS overnight at 4°C. Slides were washed in dPBS 5 \times 2 min each, followed by incubation with a goat anti-rabbit Alexafluor 594 secondary antibody (1:1000) (Invitrogen) in 20% HIGS/dPBS at room temperature in the dark for 2 hr. Slides were washed in dPBS 5 \times 2 min each, in H₂O 1 \times 2 min, and mounted with Vectamount (Vector Laboratories). Images were captured on a Zeiss Axiovert 200M microscope equipped with epifluorescence.

Dynamic light scattering

CRES^{C48A} freshly eluted off the gel filtration column at concentrations ranging from 0.17 to 0.24 mg/ml was examined by dynamic light scattering (DLS) within 2 hr of elution using a Zetasizer Nano ZS (Red) (ZEN3600, Malvern Instrument) equipped with a 633-nm red laser and 173° scattering angle, as described previously (Do et al., 2019). Other samples were examined after buffer exchange to remove NaCl and following transition to amyloid, as described above.

Thioflavin T assay

The amyloid content of CRES^{C48A} monomer and different maturational states of amyloid were determined by thioflavin T (ThT) fluorescence. Briefly, 15 μ g of each sample in 12.5 mM MES, 18.5 mM HEPES, pH 6.8, was added to a 96-well black flat-bottom plate (Corning, NY, USA) and ThT added to 20 μ M final in a final volume of 100 μ l. Fluorescence was measured using a TECAN Infinite M1000 PRO

microplate reader (Tecan Group Ltd, Männedorf, Switzerland) in the fluorescence top reading mode. The excitation and emission wavelengths were $440 \text{ nm} \pm 5$ and $485 \text{ nm} \pm 10$, respectively. ThT fluorescence was determined by averaging at least 10 reads and subtracting the ThT blank (all assay components except protein).

Statistics

Statistical analyses were performed by ANOVA followed by a Tukey or Dunnett's post-test using Graphpad Prism 9.3.1 software (GraphPad Software, San Diego, CA, USA). All data are presented as mean \pm SEM unless indicated otherwise.

Results

CRES amyloid assembly *in vitro*

We used CRES as a model for the epididymal amyloid matrix to determine if its monomer and/or amyloid forms have antimicrobial activity. To prevent inappropriate disulfide bond formation during protein expression, we modified the cysteine at position 48 in CRES to alanine (CRES^{C48A}). Full-length mouse CRES^{C48A} was purified under non-denaturing conditions from the soluble fraction of bacteria as we described previously (Do et al., 2019). Upon gel filtration, CRES^{C48A} eluted primarily as a monomer (particle diameter of $4.9 \pm 0.7 \text{ nm}$) (Fig. 1A) with also a second population of larger particles (400–800 nm) present, indicative of its propensity to aggregate (Do et al., 2019). We next exchanged the monomer into 25 mM MES, pH 6, buffer. DLS and TEM showed CRES^{C48A} had an average particle size of $4.3 \pm 0.4 \text{ nm}$ diameter and little higher ordered structure indicating it was still primarily monomeric (Fig. 1C and D). To induce amyloid assembly, CRES^{C48A} in 25 mM MES, pH 6 was concentrated to $\sim 2 \text{ mg/ml}$. In addition to monomer (average diameter $5.0 \pm 0.5 \text{ nm}$), we observed granular sheets and small assemblies of branched matrix by TEM suggesting changes in CRES^{C48A} that corresponded with early amyloid structures (Fig. 1C and D). Further adjustments of the sample to pH 6.8 (characteristic of the intraluminal pH in the caput epididymis) and concentration to $\sim 12 \text{ mg/ml}$ caused the monomer to shift to a larger particle ($6.3 \pm 0.6 \text{ nm}$ diameter), which we determined previously is a metastable oligomer (Do et al., 2019). Particles with a larger diameter ($\sim 1000 \text{ nm}$) were also detected in this sample that correlated with the appearance of larger patches of branched amyloid matrix and fragments of film (Fig. 1C and D). This sample was defined as intermediate amyloid. Finally, the sample was sonicated briefly yielding a CRES^{C48A} population that lacked monomer/oligomer and contained a highly branched amyloid matrix that structurally mimicked that which is found in the mouse caput epididymal lumen (Do et al., 2019). The sonicated sample was defined as advanced amyloid (Fig. 1C and D). Using X-ray diffraction we demonstrated previously that the advanced CRES^{C48A} amyloid exhibits cross- β -sheet architecture characteristic of amyloid (Do et al., 2019). ThT (a fluorescent dye that exhibits a spectral shift upon binding to amyloid; Biancalana and Koide, 2010) staining of the different CRES^{C48A} assemblies confirmed the presence of increased β -sheet structure in the advanced amyloid sample compared to that in monomer and early/intermediate amyloids ($P < 0.0001$) (Fig. 1B).

Amyloid forms of CRES^{C48A} have antimicrobial activity

The monomer and different maturational states of CRES^{C48A} amyloid were tested for antimicrobial activity in a CFU assay against commensal (MM294) and uropathogenic (UI012) strains of *E. coli*, the most common cause of human epididymal infections (Michel et al., 2015). The number of CFUs tested was consistent with bacteria present in human infections and in mouse models of epididymitis (Michel et al., 2016). As shown in Fig. 2A, after 2 hr incubation, the intermediate and advanced CRES^{C48A} amyloids resulted in a dose-dependent decrease in the percentage of pathogenic *E. coli* UI012 that survived compared to bacteria incubated in buffer alone (control, black bars). This effect was not seen with monomeric or early amyloid forms of CRES^{C48A}. In contrast, the survival of a commensal strain of *E. coli* MM294 was minimally affected by CRES^{C48A} (Fig. 2B). Our results show that CRES^{C48A} exhibits antimicrobial activity that is associated with its higher ordered amyloid forms. Further, our previous studies showing that similar preparations of advanced CRES^{C48A} amyloids did not decrease the viability of mouse epididymal cells in culture (Do et al., 2019) suggest the amyloids specifically affect bacteria and not mammalian host cells.

CRES^{C48A} amyloids trap bacteria and disrupt bacterial membranes

To elucidate the mechanism(s) resulting in the reduced bacterial survival (Fig. 2), we first determined if the CRES^{C48A} amyloids can trap bacteria. Commensal and pathogenic *E. coli* were stained with DAPI and then incubated with intermediate and advanced CRES^{C48A} amyloids followed by staining with the anti-amyloid antibodies A11 and OC in immunofluorescence analysis. As shown in Fig. 3A, both commensal *E. coli* MM294 and pathogenic *E. coli* UI012 bacteria (blue speckles) were trapped by the A11- and OC- labeled CRES^{C48A} amyloids (red fluorescence) forming large inclusions. The positive staining with both anti-A11 (oligomeric amyloid) and anti-OC (fibrillar amyloid) suggests several populations of CRES^{C48A} amyloids are present in the resulting structures. Bacteria incubated in the absence of CRES^{C48A} amyloid were free floating and not agglutinated (Fig. 3A). These results suggest that one host defense function of the CRES^{C48A} amyloid is the physical trapping of bacteria.

We used negative stain TEM to examine further the interactions between the advanced CRES^{C48A} amyloid and the two *E. coli* strains. After only 15 min, the advanced CRES^{C48A} amyloid matrix had attached to both strains of bacteria (Fig. 3B). The pathogenic *E. coli* UI012 were particularly affected by the CRES^{C48A} amyloid matrix, since after 2 hr the trapped cells often appeared distorted with ruffled membranes or, for some, only structures characteristic of bacterial ghosts remained (Fig. 3B) (Hjelm et al., 2015). Ghosts are nonliving empty envelopes of gram-negative bacteria that have extruded their cytoplasm and DNA but still retain a functional cell membrane that can activate a broad range of immune cells (Langemann et al., 2010). The advanced amyloid matrix also trapped the commensal *E. coli* MM294 and ghost-like structures were also occasionally detected (Fig. 3B). Our results imply that, in addition to trapping, the advanced CRES^{C48A} amyloid may kill some bacterial strains.

We next used a live/dead assay to quantify the number of bacteria that had damaged membranes and to distinguish this population from those that had formed ghost-like structures following incubation with

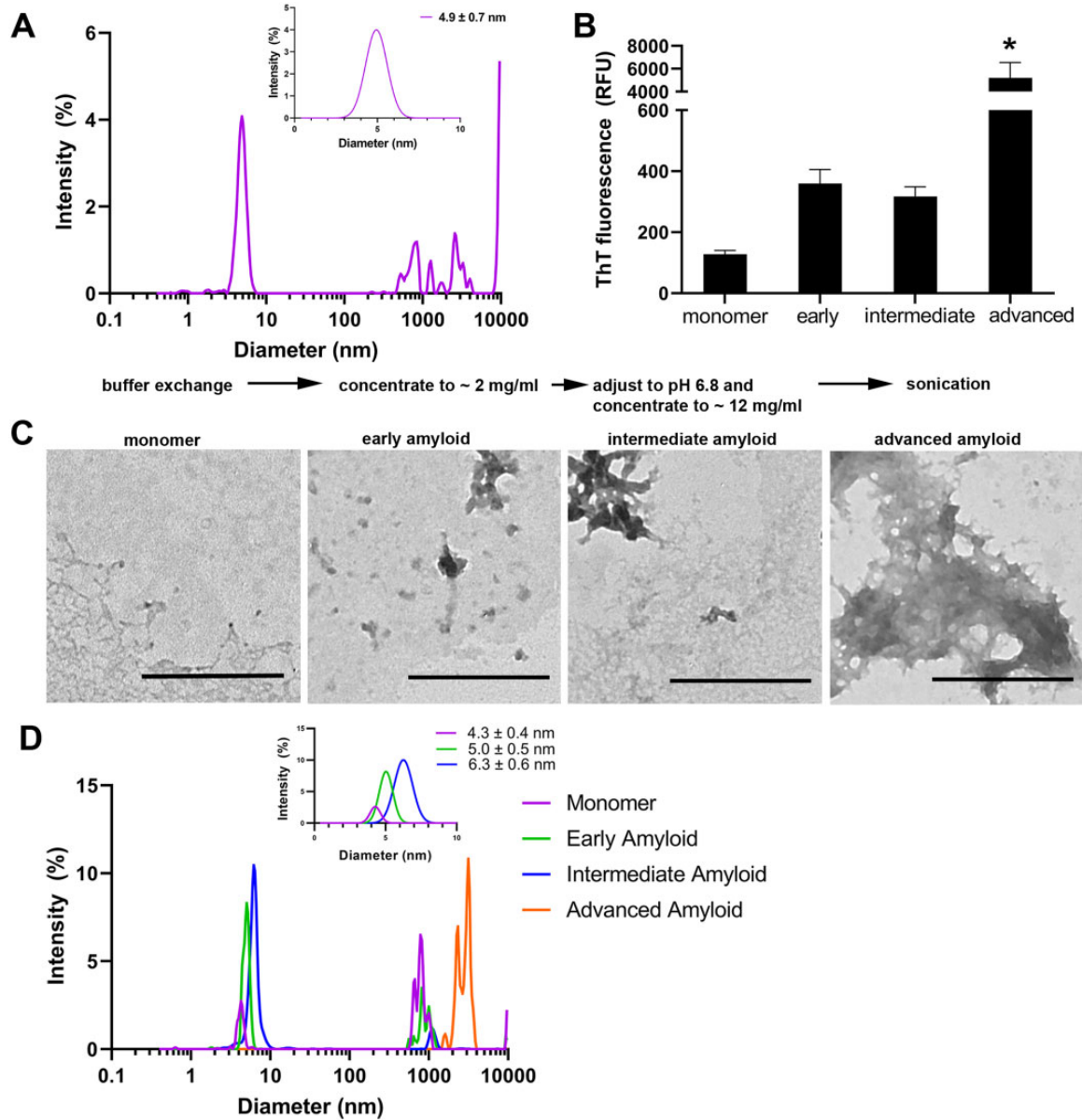


Figure 1. In vitro assembly of mouse CRES^{C48A} amyloid. (A) Dynamic light scattering (DLS) analysis of cystatin-related epididymal spermatogenic (CRES)^{C48A} freshly eluted off the gel filtration column. Intensity measurements showed populations of CRES particles at 4–8 and 400–5000 nm. Inset, an average hydrodynamic radius for the particles between 4 and 8 nm was calculated from the fitted data and diameter ± SD is reported for $n = 4$ CRES^{C48A} preparations. Owing to large variations in particle size, we were unable to fit the CRES particles between 400 and 5000 nm. (B) Thioflavin T (ThT) analysis of amyloid content in monomer, early, intermediate, and advanced CRES^{C48A} amyloid preparations. * $P < 0.001$ comparing advanced CRES^{C48A} amyloids to monomer, early, and intermediate amyloids as determined by ANOVA followed by Tukey post-test. RFU: relative fluorescence units. (C) Negative stain transmission electron microscopy and (D) DLS analysis of CRES^{C48A} monomer and different amyloid assemblies. Scale bar, 0.5 μm .

CRES^{C48A} monomer and amyloids. *E. coli* MM294 and *E. coli* UI012 were stained with DAPI (membrane permeable) and PI (membrane impermeable) and cells were imaged and counted using fluorescence microscopy. Representative staining patterns of the bacteria are shown in Supplementary Fig. S1. Bacteria with disrupted membranes were

DAPI positive/PI positive (faint or strong). Bacterial ghost-like structures were identified by their faint DAPI staining, often at the cell periphery, and no PI fluorescence or strong DAPI stained dense bodies at their septum or poles, and no PI fluorescence (Supplementary Fig. S1). The intermediate and advanced CRES^{C48A} amyloids, but not the

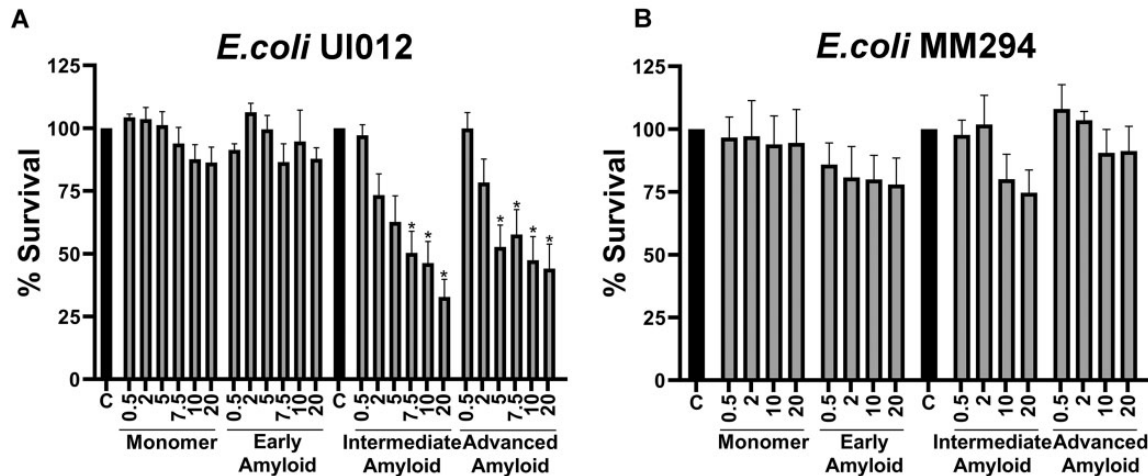


Figure 2. Mouse CRES^{C48A} amyloids decrease pathogenic *E. coli* survival. Colony-forming unit (CFU) assays show the percentage of (A) pathogenic *Escherichia coli* UI012 and (B) commensal *E. coli* MM294 that survived following a 2 hr incubation with increasing concentrations (0.5–20 μg/ml) of cystatin-related epididymal spermatogenic (CRES)^{C48A} monomer and amyloids. C, Control samples of bacteria incubated in buffer only. Buffer for monomer and early amyloid was 25 mM MES, pH 6. Buffer for intermediate and advanced amyloid was 18.75 mM MES, 12.5 mM HEPES, pH 6.8. The number of CFUs in the control samples was set to 100%. Values shown are the mean ± SEM of 6–8 replicate experiments using 6–8 different CRES^{C48A} preparations. **P* < 0.0001–0.0117 compared to control as determined by ANOVA followed by Tukey post-test.

monomeric or early amyloids, reduced the percentage of pathogenic *E. coli* UI012 that had intact membranes suggesting CRES^{C48A} is bactericidal against this strain (Fig. 3C). Although not as profound as observed with *E. coli* UI012, *E. coli* MM294 also showed decreased membrane integrity in the presence of intermediate and advanced amyloids (Fig. 3E). This outcome was different from the CFU assay in which no change in *E. coli* MM294 bacterial survival was noted across all CRES^{C48A} populations (Fig. 2B). Because more *E. coli* (10⁴) were needed to perform the live/dead assay, a more pronounced response from CRES^{C48A} may have occurred. We also cannot rule out the possibility that membrane integrity was reduced due to a fast exponential growth of these cells (Berney et al., 2007). A small percentage of pathogenic and commensal *E. coli* formed ghost-like structures in the presence of CRES^{C48A} amyloid (Fig. 3D and F). However, only the pathogenic *E. coli* UI012 showed a significant increase in the percentage of ghost-like structures compared to control (buffer only) bacteria (Fig. 3D).

Commensal and pathogenic bacteria induce changes in CRES^{C48A} structure

Some antimicrobial proteins assemble into amyloid only after their interaction with bacteria, as a means to trap or trap and kill the pathogen (Brinkmann et al., 2004; Chu et al., 2012). To determine if bacteria induce changes in CRES^{C48A}, monomer was incubated with commensal and pathogenic *E. coli* and structural changes were monitored by TEM after 15 min and 2 hr. In the absence of bacteria, the few visible structures in the CRES^{C48A} monomer in buffer alone (control) exhibited minimal change over the time course (Fig. 4A, B, C and D). The addition of bacteria, however, caused a profound change in

CRES^{C48A} monomer that varied with the bacterial strains and time. Following 15 min incubation with the commensal *E. coli* MM294, film fragments were detected in the CRES^{C48A} monomer that often extended fibrils to the bacterial surface (Fig. 4E and F). In contrast, after 2 hr, assemblies of branched matrix were prevalent and included populations that were attached to and trapped the bacteria (Fig. 4G and H). Incubation of CRES^{C48A} monomer with the pathogenic *E. coli* UI012 similarly resulted in the appearance of film fragments (Fig. 4I and K); however, broad arrays of fibrils were associated with the bacterial surface while little to no matrix was present (Fig. 4J and L). Further, ghost-like structures were common and often had fibrils associated with their surface (Fig. 4J and L). Our studies suggest the commensal and pathogenic *E. coli* promoted aggregation in a strain-dependent manner with CRES^{C48A} assembling into its characteristic branched matrix (Do et al., 2019) in the presence of commensal *E. coli* but forming fibrils with the pathogenic *E. coli*. Although none of the amyloid structures were present in samples of bacteria incubated in buffer alone we cannot eliminate the possibility that some assemblies were generated by the bacteria in response to CRES^{C48A} as bacteria also use amyloid as a host defense mechanism (Schwartz and Boles, 2013).

The epididymal amyloid matrix has antimicrobial activity

Having shown that CRES^{C48A} amyloids are antimicrobial (Figs 2, 3 and 4), we next wanted to determine whether the endogenous mouse epididymal amyloid matrix (which contains CRES and other CRES subgroup members) also has antimicrobial activity. As shown schematically in Fig 5A, the epididymis is a single, long, highly coiled

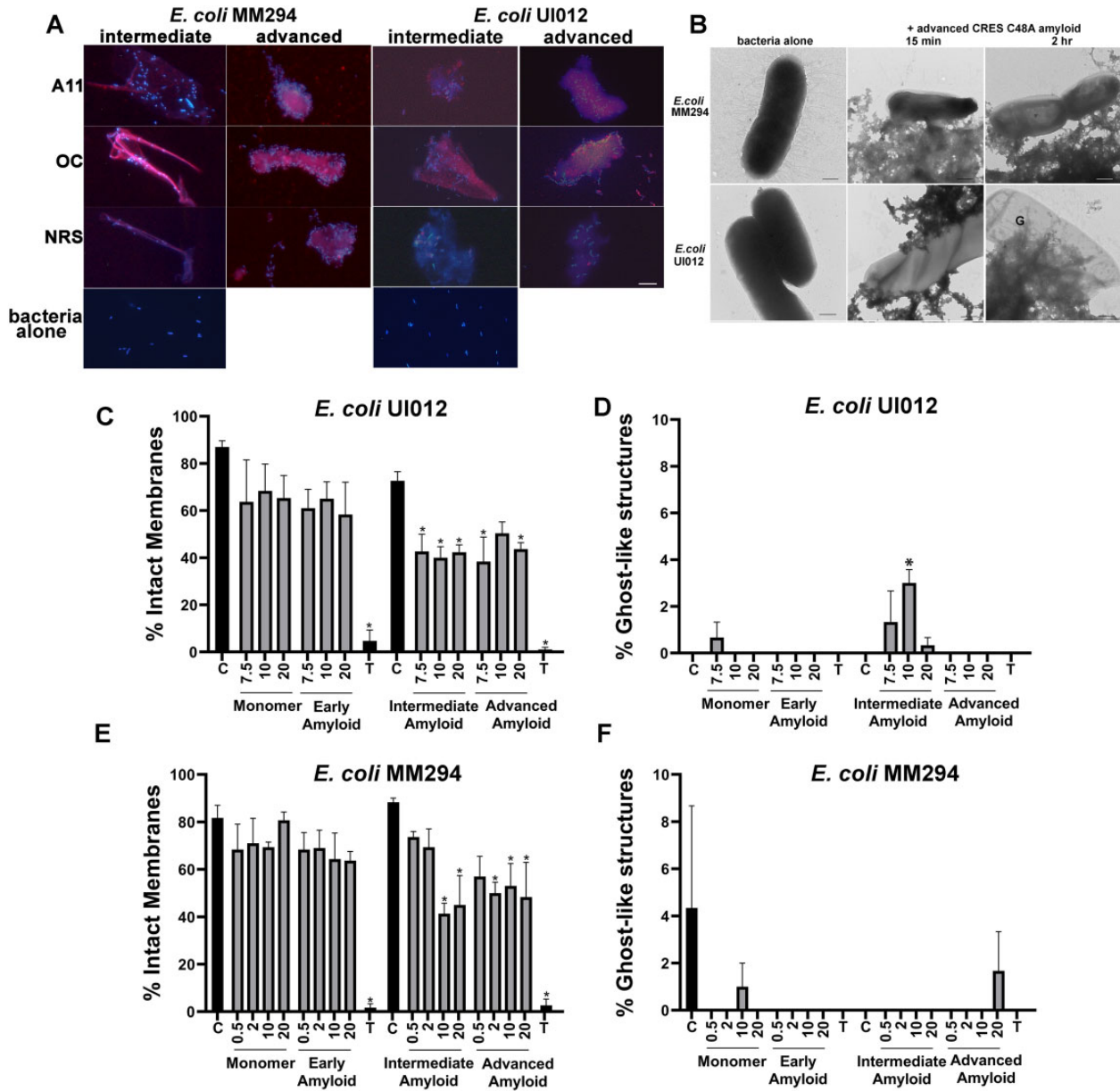


Figure 3. Antimicrobial mechanisms of the mouse CRES^{C48A} amyloids. (A) *Escherichia coli* MM294 and UI012 were labeled with DAPI and incubated with intermediate and advanced cystatin-related epididymal spermatogenic (CRES)^{C48A} amyloids for 15 min. Samples were spread on a slide and incubated with the anti-amyloid antibodies A11 and OC or normal rabbit serum (NRS, negative control) in immunofluorescence analysis. The merged images of DAPI (blue) and Alexa 594 (red) fluorescence reveal bacteria are trapped by CRES^{C48A} amyloid. Scale bar all images, 0.2 μm. (B) Advanced CRES^{C48A} amyloids were incubated with 10⁴ CFUs *E. coli* MM294 and *E. coli* UI012 for 15 min and 2 hr after which the samples were examined by negative stain transmission electron microscopy. Scale bar, 0.5 μm. G, Bacterial ghost-like structure. (C–F) Live/dead assays were performed following incubation of bacteria with increasing concentrations (0.5–20 μg/ml) of CRES^{C48A} monomer and amyloids and the percentage of bacteria with intact membranes and ghost-like structures are shown. C, Control bacteria incubated in buffer only. Buffer for monomer and early amyloid was 25 mM MES, pH 6. Buffer for intermediate and advanced amyloid was 18.75 mM MES, 12.5 mM HEPES, pH 6.8. The number of bacteria with intact membranes in the control samples was set to 100%. Representative DAPI and propidium iodide staining patterns of healthy, membrane damaged, and ghost-like structures are shown in [Supplementary Fig. S1](#). Values shown are the mean ± SEM of three replicate experiments using three different CRES^{C48A} preparations. **P* < 0.0001–0.0103 compared to control as determined by ANOVA followed by Dunnett's post-test.

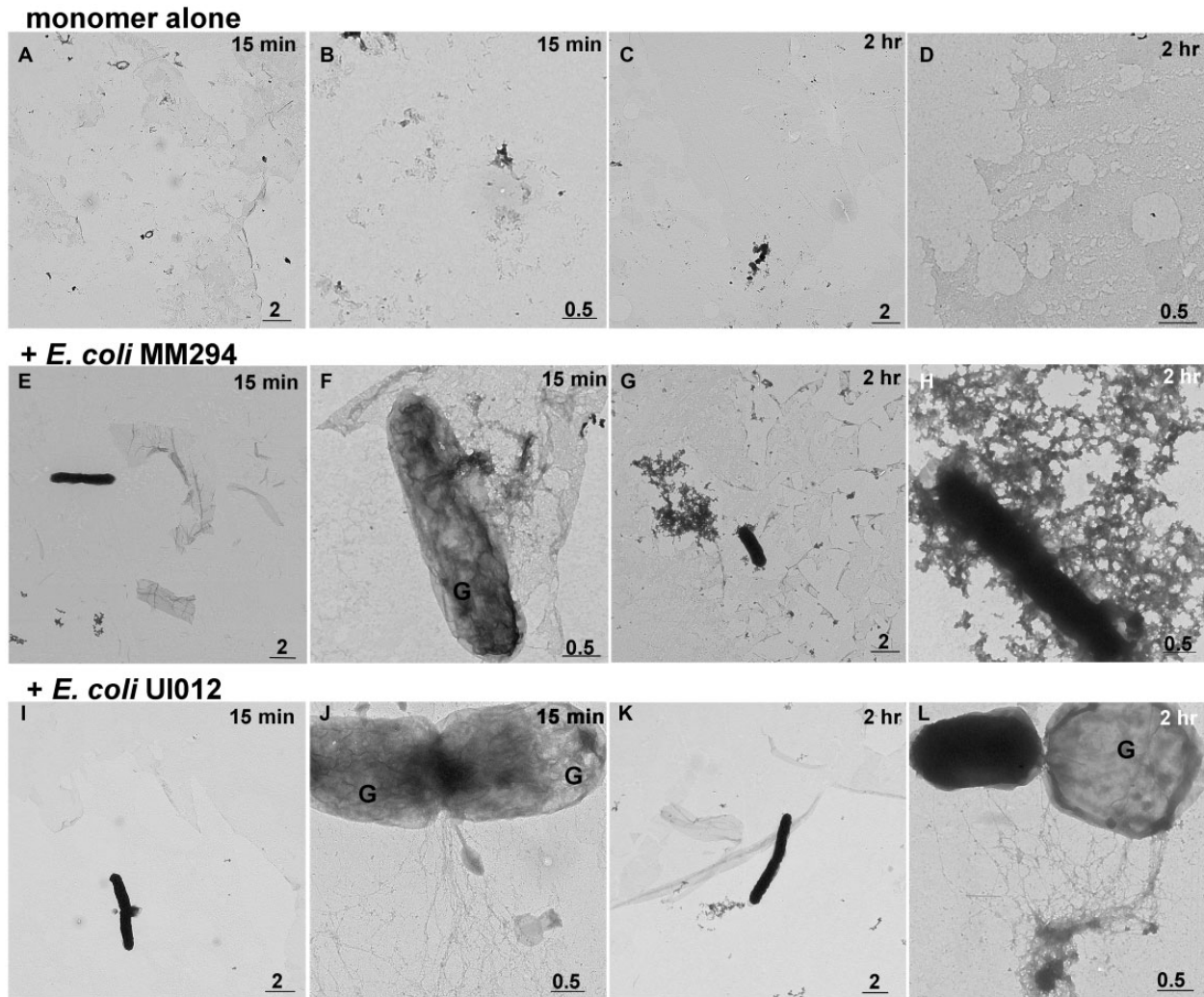


Figure 4. Changes in mouse CRES^{C48A} monomer in the presence of bacteria. Cystatin-related epididymal spermatogenic (CRES)^{C48A} (20 μg/ml) monomer was incubated with 10⁴ bacteria for 15 min and 2 hr, samples were pelleted and then dried on to Formvar/carbon-coated 200 mesh nickel grids for analysis by negative stain transmission electron microscopy. G, ghost-like structure. Scale bar, 0.5 or 2 μm as indicated. Images are representative of three experiments.

tubule that connects the testis to the vas deferens and which functionally matures and protects the spermatozoa as they migrate from the proximal/caput to the distal/cauda part of the tubule. CRES, CRES2, CRES3 and cystatin E2 are synthesized by the epithelium in the caput epididymis and secreted into the lumen where they are components of the assembling amyloid matrix (Whelley et al., 2016). The amyloid matrix changes along the length of the epididymal tubule, transitioning from a highly branched structure in the caput epididymis to mostly fibrillar in the corpus-cauda epididymis (Supplementary Fig. S2). We used differential centrifugation to isolate the epididymal amyloids (pellet fractions P2, P4) from the caput and corpus-cauda epididymal lumen (Fig. 5B and Supplementary Fig. S2). Previously, in addition to using anti-amyloid antibodies (A11, OC), we used conformation-dependent dyes Thioflavin S and Congo Red and X-ray diffraction to

demonstrate that the caput and corpus-cauda P2 and P4 pellet fractions contain cross-β-sheet-rich amyloids (Whelley et al., 2012, 2016).

To determine if the epididymal amyloids have antimicrobial activity along the length of the epididymal tubule, the P2 and P4 amyloid-containing fractions from the caput and corpus-cauda epididymis were incubated with the two bacterial strains and CFU assays were performed as described for CRES^{C48A} amyloids. The P2 and P4 fractions from the caput and corpus-cauda caused a dose-dependent decrease in the survival of the commensal (Fig. 5C) and pathogenic strain of *E. coli* (Fig. 5D), with a more robust effect observed against the commensal strain. Together, our results show that the endogenous amyloids (P2 and P4 fractions) from the caput and cauda epididymis have antimicrobial activity but that their effectiveness varies depending on the bacterial strain. We cannot rule out that other structures such as

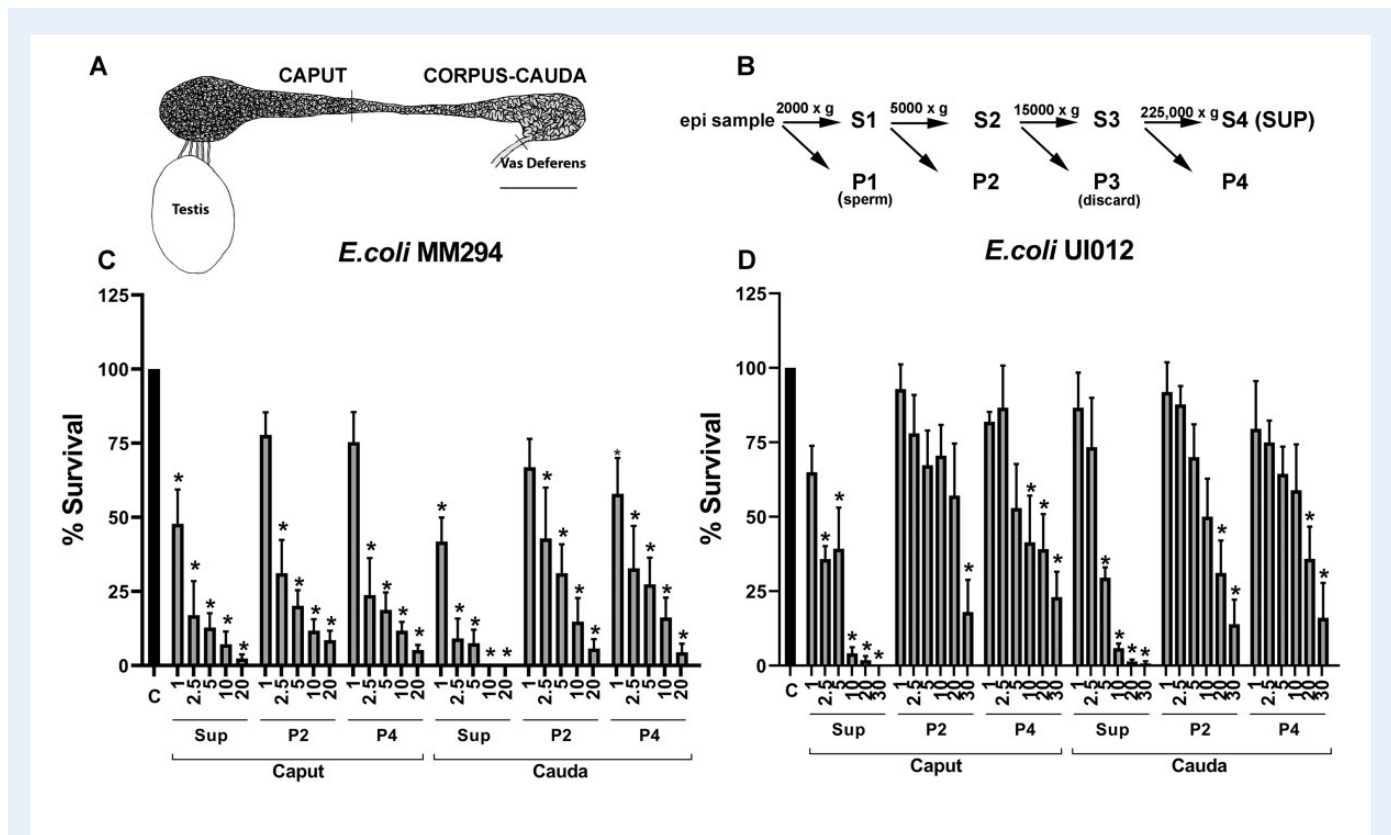


Figure 5. The mouse epididymal amyloid-containing fractions decrease *Escherichia coli* survival. (A) Schematic diagram of the rodent epididymis showing the caput and corpus-cauda regions and its connections to the testis and vas deferens. Scale bar, 3 mm. (B) Differential centrifugation protocol used to isolate amyloids of different molecular mass from the caput and corpus-cauda epididymal lumen. S, supernatant; P, pellet. The P3 pellet contained little thioflavin S positive material and was not studied further. Colony-forming unit (CFU) assays show the percentage of (C) *E. coli* MM294 and (D) *E. coli* UI012 that survived following a 2 hr incubation with increasing concentrations (1–30 µg/ml) of the P2 and P4 amyloid fractions and final supernatant (SUP, S4) fraction from the caput and corpus-cauda epididymis. C: control, bacteria incubated in buffer only. The number of CFUs in the control samples was set to 100%. Values shown are the mean \pm SEM of 4–6 replicate experiments using 4–6 different epididymal amyloid preparations. * $P < 0.0001$ – 0.0128 compared to control as determined by ANOVA followed by Tukey post-test.

extracellular vesicles/exosomes (EVs) that may pellet with the epididymal amyloids contribute to the antimicrobial activity. Indeed, we have shown previously that populations of CRES subgroup members are associated with EVs (Whelly *et al.*, 2016). The final supernatant (SUP, S4), resulting from the high-speed centrifugation to generate pellet 4 (Fig. 5B) and representing the soluble fraction from the caput and corpus-cauda, also exhibited robust antimicrobial activity against the *E. coli* strains. This activity likely reflects the antimicrobial actions of other AMPs that are present in the epididymal lumen such as defensins (Hall *et al.*, 2007) and/or soluble oligomeric forms of antimicrobial amyloids.

Caput and corpus-cauda epididymal amyloids trap bacteria and undergo structural changes

To determine a mechanism for the antimicrobial activity of the epididymal amyloids against the *E. coli* strains, we first used TEM to examine their interactions. Similar interactions/structures were noted after 15 min and 2 hr coinoculation and therefore only the 2 hr time points

are shown. Epididymal amyloid from the caput and corpus-cauda P2 and P4 fractions attached to and surrounded the bacteria suggesting that, like CRES^{C48A}, one host defense response is to trap the bacteria (Fig. 6). Further, the epididymal amyloids often underwent structural changes in the presence of bacteria. Specifically, spherical structures that are prevalent in the caput and corpus-cauda P2 fractions and that may be early condensates/assemblies (Fig. 6A, C, E and G and Supplementary Fig. S2), coalesced and transitioned into dense matrices that surrounded and trapped the commensal *E. coli* MM294 (Fig. 6B and D). A similar coalescence of spheres occurred in the presence of *E. coli* UI012. However, compared to the commensal strain, the assemblies were smaller and ghost-like structures were frequently observed (Fig. 6F and H).

The highly branched matrix and films typical of caput P4 amyloid (Supplementary Fig. S2), became a thin matrix/film after dilution in the assay buffer (control), suggesting some disassembly (Fig. 6I and M). However, following the addition of *E. coli* MM294, dense matrices and thick films that trapped bacteria were observed (Fig. 6J). In contrast, matrix was rarely detected following incubation of caput P4 amyloid with *E. coli* UI012 but bacteria were often ghost-like (Fig. 6N). In the

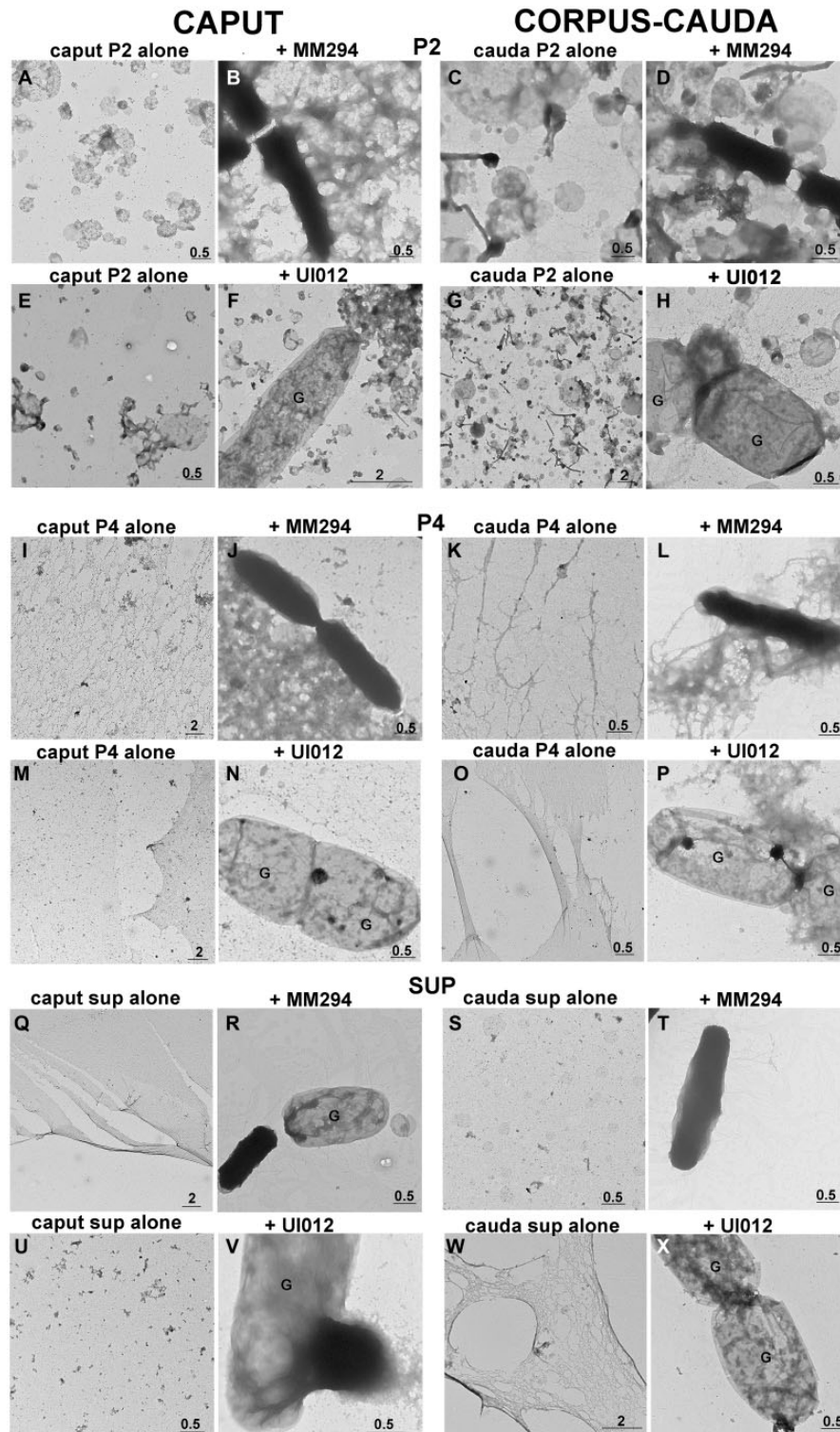


Figure 6. Host defense responses of the caput and corpus-cauda epididymal amyloids. Pellet 2 and pellet 4 (P2, P4) and final supernatant (SUP, S4) fractions (20 $\mu\text{g}/\text{ml}$) from the mouse caput and corpus-cauda epididymis were incubated with 10^4 *Escherichia coli* MM294 and *E. coli* UI012 for 2 hr, after which samples were pelleted and dried onto grids for analysis by negative stain transmission electron microscopy. Epididymal amyloids incubated in buffer only served as controls. Scale bar, 0.5 or 2 μm as indicated. G, bacterial ghost-like structure. Based on DAPI stained images in [Supplementary Fig. S1](#), we speculate the dense body associated with the bacterium in panel **V** is extruded DNA/cytosol. Images are representative of two experiments.

corpus-cauda epididymis, the thin fibrils and matrix typical of the P4 amyloid (Supplementary Fig. S2) trapped both commensal and pathogenic *E. coli* in thin film-like webs and occasionally in fibrillar matrices (Fig. 6L and P); however, ghost-like structures were more often detected in the pathogenic *E. coli* UI012 samples (Fig. 6P).

The supernatants (SUP, S4), which represent the soluble fraction of the epididymal fluid, contained few structures except for individual spheres, which may be very early condensates, small particles and the occasional thin or branched matrix (Fig. 6Q, S, U and W and Supplementary Fig. S2). Commensal and pathogenic *E. coli* incubated with the caput and corpus-cauda SUP appeared intact (Fig. 6T), or were observed transitioning into (Fig. 6V), or had already formed ghost-like structures (Fig. 6R and X). The ghost-like structures were detected more often in the pathogenic *E. coli* UI012 compared to the commensal strain. Together, our TEM results show the epididymal amyloids undergo structural changes in the presence of bacteria, often forming more advanced assemblies (spheres to matrix, increased matrix) that trap the pathogen. The structures that formed, however, varied between the commensal and pathogenic *E. coli* strains. It is possible that local disassembly of the epididymal amyloids may also occur in response to bacteria.

Epididymal amyloids disrupt *E. coli* membranes and promote ghost-like structures

As performed with CRES^{C48A}, we used the live/dead assay to quantify the number of bacteria that had disrupted membranes and those that had formed ghost-like structures following incubation with the epididymal amyloids. As shown in Fig. 7A, all epididymal amyloid-containing fractions caused a significant decrease in the percentage of pathogenic *E. coli* UI012 that had intact membranes compared to control bacteria incubated in buffer alone. In contrast, only the highest concentrations of caput P2 and P4 amyloid fractions were effective at disrupting the bacterial membranes of the commensal *E. coli* MM294 while the other epididymal amyloid populations showed little effect (Fig. 7C). In addition, ghost-like structures were prevalent in *E. coli* UI012 after incubation with the epididymal amyloid populations, especially in the P4 amyloid and soluble/supernatant fractions (Fig. 7B), confirming our results by TEM (Fig. 6). In contrast, fewer ghost-like structures were detected in the commensal *E. coli* MM294 (Fig. 7D).

Discussion

Host defense functions of the epididymal amyloid matrix

Our studies reveal a functional role for the epididymal amyloid matrix in host defense. We show that the different epididymal amyloid-containing fractions and CRES^{C48A} amyloids exhibit potent antimicrobial activity against commensal and pathogenic strains of *E. coli*, the most common causes of epididymal infections in men (Pilatz et al., 2015). Epididymitis is usually caused by the ascent of bacteria in the urogenital tract, with pathogens originating from urinary tract infections or sexually transmitted diseases (Michel et al., 2015). In addition to *E. coli*, other common pathogens that cause epididymal infections are *Chlamydia trachomatis*

and *Neisseria gonorrhoeae* but also can include *Pseudomonas aeruginosa*, *Staphylococcus aureus* and others (Michel et al., 2015).

Our studies show the epididymal amyloids and CRES^{C48A} amyloids use several antimicrobial mechanisms to protect the host. Both the P2 and P4 epididymal amyloid fractions and the advanced CRES^{C48A} amyloids, represented by an amyloid matrix, rapidly attached to and surrounded the bacteria suggesting that trapping is an initial and perhaps primary mode of defense. Furthermore, CRES^{C48A} monomer and P2 amyloids transitioned into matrix in the presence of bacteria indicating bacterial membranes may function as biological templates to facilitate the assembly of immature amyloids into functional structures to enable trapping. This is not unlike several other antimicrobial amyloids such as the α -defensin HD6 in the gut that assembles into nanonets only after encountering the pathogen (Chu et al., 2012). Whether the P2 structures represent early maturational states of amyloid that will ultimately assemble into matrix or fibrils or are structures that normally exist in equilibrium with the advanced amyloid forms within the epididymal lumen is not known. The caput P4 amyloid, and to a lesser degree the corpus-cauda P4 amyloid, also underwent structural transitions in the presence of bacteria to facilitate trapping although the changes observed varied depending on the pathogen.

The epididymal amyloid-containing fractions and CRES^{C48A} amyloids also disrupt bacterial membranes (Figs 3 and 7). In particular, pathogenic *E. coli* were affected more than the commensal strain suggesting CRES^{C48A} and the epididymal amyloids elicit different responses depending upon the strain of bacteria or pathogen. The trapping of bacteria by the epididymal amyloids involved multiple points of association with the membrane that could lead to a generalized disruption. The promotion of ghost-like structures (Figs 6 and 7), however, is likely the result of membrane damage by a different mechanism as these cells remained impervious to PI, a membrane impermeable dye (Fig. 7 and Supplementary Fig. S1). Ghosts have been observed in gram-negative bacteria after their infection with bacteriophage Φ X174 and are caused by the expression of a phage lysis protein that oligomerizes to form a single lysis tunnel in the bacterial membrane (Witte and Lubitz, 1989). Our studies show that mammalian amyloids promote structures that resemble bacterial ghosts. We have not determined if the inner and outer membranes fused to form a lysis tunnel in the ghost-like bacteria that we observed and thus cannot conclude that they are ghosts. However, the ghost-like structures exhibited DNA positive dense bodies at potential cell division sites (center or poles) on the bacterial surface, sites where DNA and cytosol are extruded and hallmarks of lysis tunnel formation (Fig. 6V and Supplementary Fig S1) (Witte et al., 1992). Together, our data indicate that the bactericidal properties of CRES^{C48A} and the epididymal amyloids are likely a result of several different mechanisms that may be determined by the maturational state of the amyloid as well as the pathogen they encounter.

The strain-specific host defense responses of the epididymal and CRES^{C48A} amyloids mimic human infections

Human epididymitis induced by different pathogenic bacterial infections has different characteristics. Infection with pathogenic strains of *E. coli* often results in luminal occlusions while infection with commensal strains of *E. coli* do not, suggesting distinct host defense responses within the

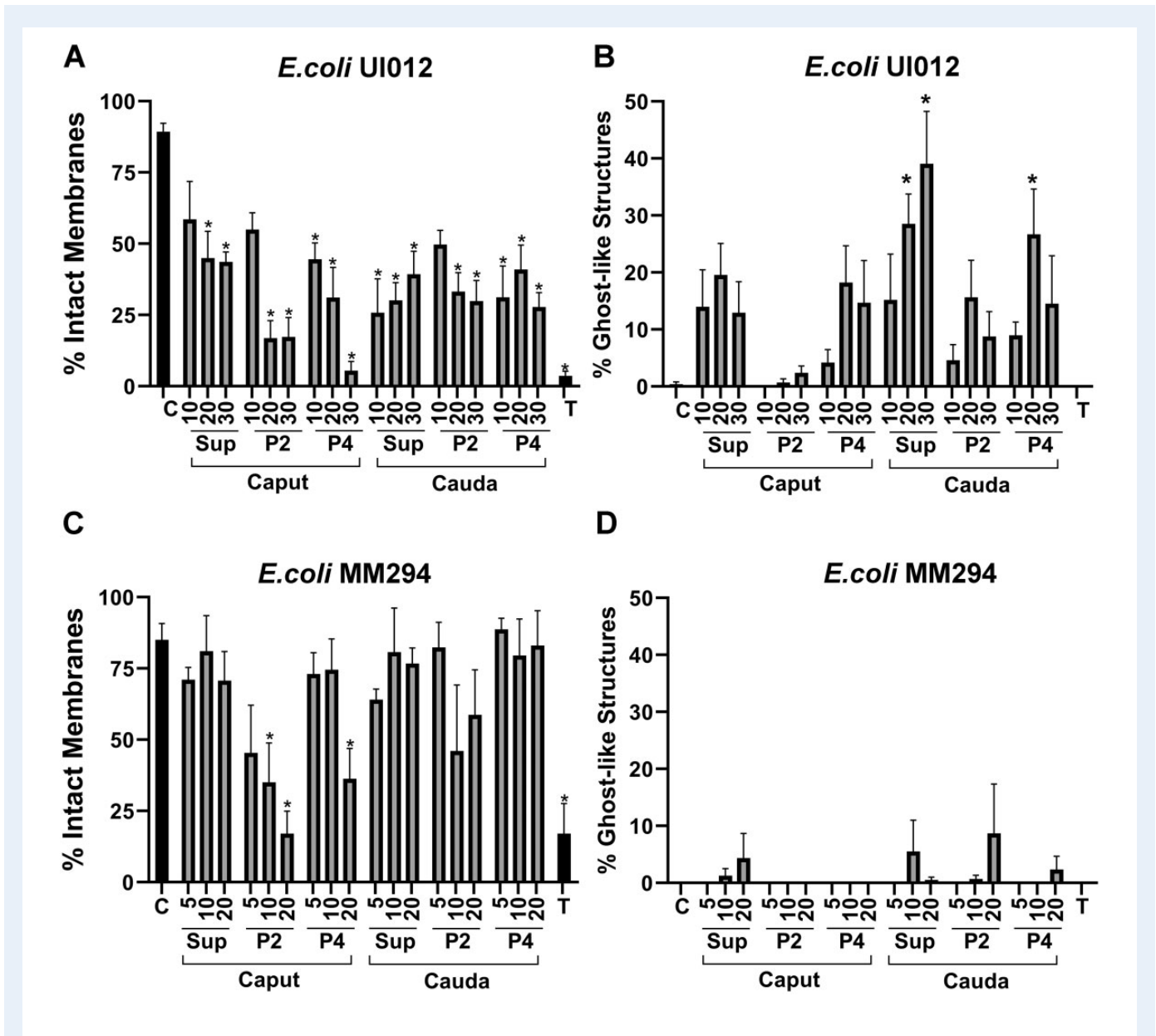


Figure 7. Mouse epididymal amyloid-containing fractions disrupt *Escherichia coli* membranes and promote bacterial ghost-like structures in a strain-dependent manner. Live/dead assays were performed to determine bacterial membrane integrity and the induction of bacterial ghost-like structures following a 2 hr incubation of (A and B) *E. coli* UI012 and (C and D) *E. coli* MM294 with increasing concentrations (0.5–30 $\mu\text{g}/\text{ml}$) of the pellet 2 (P2) and P4 amyloid fractions and final supernatant (SUP, S4) from the caput and corpus-cauda epididymis. Representative DAPI and propidium iodide staining patterns of healthy, membrane damaged, and ghost-like structures are shown in Supplementary Fig. S1. Values represent mean \pm SEM of 3–5 replicate experiments. C, control samples of bacteria incubated in buffer only; T, bacteria incubated in 1% Triton X-100 (positive control). * $P < 0.0001$ – 0.0483 compared to control as determined by ANOVA followed by Dunnett's post-test.

human epididymal lumen (Michel et al., 2016). Indeed, up to 40% of men who have recovered from an infection with a pathogenic *E. coli* strain still exhibit oligospermia and infertility, possibly owing to sperm obstruction as a result of the epididymal occlusion. Similar *E. coli* strain-specific phenotypes have been recapitulated in a mouse model for human epididymitis (Lang et al., 2013). The mechanisms that underlie these pathogen-specific responses, including the events that lead to the

formation of luminal occlusions, are not well understood. Our studies show that $\text{CRES}^{\text{C48A}}$ amyloid and the epididymal amyloids responded differently to the commensal and pathogenic *E. coli* stains *in vitro* suggesting the same may occur within the epididymal lumen and possibly contribute to the diverse characteristics of human epididymal infections. Collectively our data show the epididymal amyloids and $\text{CRES}^{\text{C48A}}$ assembled into dense matrices that trapped but minimally killed the

commensal *E. coli* MM294. In contrast, fewer assemblies surrounded the pathogenic *E. coli* UI012 but bactericidal activity was significant and included the prevalence of ghost-like structures (summarized in [Supplementary Table S1](#)). Because bacterial ghosts are highly immunogenic, they may activate distinct and robust innate and adaptive immune responses, such as toll-like receptors and downstream proinflammatory responses, which are not, or only minimally activated, with the commensal strain, leading to inclusions within the epididymal lumen. In our studies, the bacterial ghost-like structures were especially numerous in epididymal amyloid and supernatant fractions from the corpus-cauda epididymis as compared to the caput, indicating that host defense responses within the epididymis may vary between regions. Our observations are consistent with what happens in human epididymal infections wherein the cauda elicits a stronger immune response and inflammatory damage compared to the caput region ([Pleuger et al., 2020](#)). Future studies using a mouse model for epididymitis will help establish the contributions of the epididymal amyloid matrix to these pathogen- and region-specific phenotypes.

The transition of CRES^{C48A} monomer and immature epididymal amyloids to advanced assemblies following exposure to the bacteria may be a reaction to specific virulence factors the bacteria release and/or components associated with their surface/membrane. *E. coli* and other gram-negative strains possess lipopolysaccharide in their membranes, a toxin that can activate host immune responses including inducing some AMPs to assemble into amyloid ([Wang et al., 2014](#)). Other proteins and peptides assemble into amyloid directly from their interactions with membrane lipids ([Soria et al., 2017](#); [Gu and Guo, 2021](#)). Gram-negative and some gram-positive bacteria possess pili and fimbriae that function in cell migration and adhesion but which are also virulence factors and in some bacteria are amyloids that can interact with mammalian amyloidogenic AMPs ([Kai-Larsen et al., 2010](#)). The contributions of one or several of these bacterial factors could lead to the structural changes in CRES^{C48A} and the epididymal amyloids.

A new host defense amyloid

Our studies showing the epididymal amyloid matrix is a host defense structure broadens the list of antimicrobial amyloids that exist in nature to include a sophisticated amyloid scaffold that functions to protect the male germline ([Kagan et al., 2012](#)). We show the epididymal amyloid matrix is exquisitely sensitive to pathogens, adopting different conformations and using distinct host defense mechanisms depending on the bacterial strain that is present. Whether strain-specific host defense responses are unique to the epididymal amyloid matrix or also a characteristic of other host defense amyloids is not known. However, the presence of CRES and other amyloidogenic CRES subgroup family members within the epididymal amyloid matrix may contribute to its fluidity. Indeed, our studies here show that CRES carries out its antimicrobial functions as an amyloid, forming distinct structures and eliciting strain-specific effects on bacteria, similar to that of the endogenous amyloid matrix. In previous studies, we determined that CRES can assemble into amyloid via several different pathways ([Hewetson et al., 2020](#)), which could be influenced by the local environment, such as bacterial virulence factors, and allow different conformations/functions. While we have yet to establish if other CRES subgroup members also

exhibit antimicrobial activity as amyloids, their presence within the amyloid matrix could allow the formation of distinct β -sheet assemblies further contributing to a robust and plastic antimicrobial structure. Based on our observations, we speculate the maturational state of the epididymal amyloid matrix (caput versus corpus-cauda, P2 versus P4 amyloids), the pathogen it encounters and its repertoire of secreted and surface-associated virulence factors, and possibly local pathogen load, may influence the host defense response. As we show with CRES^{48A} monomer and the epididymal amyloids, a response was often the transition of immature structures into more advanced forms (matrix, films and fibrils). However, it is also possible that the epididymal amyloids disassemble to generate soluble oligomeric conformers that could create tunnels or pores in bacterial membranes, potentially promoting bacterial ghosts ([Di Scala et al., 2016](#)).

It is of interest that other AMPs and proteins in the epididymal lumen are also prone to aggregation. These include the LL-37 peptide of cathelicidin hCAP-18 (mouse CAMP), a potent AMP that self-assembles into helical fibrils structurally similar to the cross- α amyloids of the *S. aureus* phenol soluble modulins PSM α 3 peptide ([Engelberg and Landau, 2020](#)), lactoferrin ([Nilsson and Dobson, 2003](#)) and lysozyme ([Booth et al., 1997](#)). The β -sheet-rich defensins also may also form amyloid for their antimicrobial actions, similar to some α -defensins such as HD6 ([Chu et al., 2012](#)). Thus, while some AMPs in the epididymal lumen are soluble, as indicated by the antimicrobial activity in the supernatant fractions, it is possible that other aggregation-prone epididymal AMPs contribute to the assembly of, or are attached to, the epididymal amyloid matrix possibly via cross- α and cross- β -sheet interactions. Such a highly integrated scaffold could further expand the potential for distinct assemblies to form as needed in order to respond to a diverse repertoire of pathogens and also provide a means to coordinate multiple host defense responses following an infection, including the activation of downstream immune responses.

Finally, because the epididymal amyloid matrix is constitutively expressed and dispersed throughout the lumen intertwined with the maturing spermatozoa, we think it likely it also carries out critical roles in sperm maturation. Several epididymal AMPs and proteins, including β -defensins, lactoferrin, EPPIN, lysozyme and lysozyme-like protein 6, SPAG11 isoforms and others, have dual functions. In addition to their antimicrobial roles, they bind to spermatozoa and affect their function, including fertilizing ability, in both rodent models and humans ([Jin et al., 1997](#); [Yenugu et al., 2004](#); [Zhou et al., 2004](#); [Wei et al., 2013](#); [Huang et al., 2017](#)). Similarly, cathelicidin, CRES, CRES2 and CRES3 bind to epididymal spermatozoa for reasons not yet known ([Malm et al., 2000](#); Cornwall, unpublished observations). Perhaps by integrating multifunctional AMPs, antimicrobial proteins and possibly other proteins into a common yet sophisticated amyloid scaffold the epididymis has devised a way to integrate its two critical functions of sperm maturation and protection.

Supplementary data

Supplementary data are available at *Molecular Human Reproduction* online.

Data availability

All data are contained within the article.

Acknowledgements

The authors gratefully acknowledge Abdul Hamood, Ph.D., TTUHSC for his generous sharing of bacterial isolates and helpful comments and suggestions and Stephany Navarro, M.S., TTUHSC for her assistance with the CFU and biofilm assays. The authors also thank Jannette Dufour, Ph.D., Clint MacDonald, Ph.D., and R. Bryan Sutton, Ph.D. TTUHSC for their critical reading of the article.

Authors' roles

C.M. and G.A.C. designed the experiments, C.M., M.C.H., and G.A.C. performed the experiments and analyzed the data, and C.M. and G.A.C. wrote the paper. All authors approved the final version of the article.

Funding

TTUHSC and The Newby Family (to G.A.C.). The funders had no role in the study design, data collection and interpretation or preparation and reporting of the study.

Conflict of interest

The authors declare that they have no conflicts of interest with the contents of this article.

References

- Berney M, Hammes F, Bosshard F, Weilenmann HU, Egli T. Assessment and interpretation of bacterial viability by using the LIVE/DEAD BacLight kit in combination with flow cytometry. *Appl Environ Microbiol* 2007;**73**:3283–3290.
- Biancalana M, Koide S. Molecular mechanism of Thioflavin-T binding to amyloid fibrils. *Biochim Biophys Acta* 2010;**1804**:1405–1412.
- Booth DR, Sunde M, Bellotti V, Robinson CV, Hutchinson WL, Fraser PE, Hawkins PN, Dobson CM, Radford SE, Blake CCF et al. Instability, unfolding and aggregation of human lysozyme variants underlying amyloid fibrillogenesis. *Nature* 1997;**385**:787–793.
- Brinkmann V, Reichard U, Goosmann C, Fauler B, Uhlemann Y, Weiss DS, Weinrauch Y, Zychlinsky A. Neutrophil extracellular traps kill bacteria. *Science* 2004;**303**:1532–1535.
- Chu H, Pazgier M, Jung G, Nuccio S-P, Castillo PA, de Jong MF, Winter MG, Winter SE, Wehkamp J, Shen B et al. Human alpha-defensin 6 promotes mucosal innate immunity through self-assembled peptide nanonets. *Science* 2012;**337**:477–481.
- Cornwall GA, Cameron A, Lindberg I, Hardy DM, Cormier N, Hsia N. The cystatin-related epididymal spermatogenic protein inhibits

- the serine protease prohormone convertase 2. *Endocrinology* 2003;**144**:901–908.
- Di Scala C, Yahi C, Boutemour N, Flores S, Rodriguez A, Chahinian L, Fantini H. J. Common molecular mechanism of amyloid pore formation by Alzheimer's beta-amyloid peptide and alpha-synuclein. *Sci Rep* 2016;**6**:28781.
- Do HQ, Hewetson A, Myers C, Khan NH, Hastert MC, Harsini FM, Latham MP, Wylie BJ, Sutton RB, Cornwall GA. The functional mammalian CRES (Cystatin-Related Epididymal Spermatogenic) amyloid is antiparallel beta-sheet rich and forms a metastable oligomer during assembly. *Sci Rep* 2019;**9**:9210.
- Eaves-Pyles T, Patel J, Arigi E, Cong YZ, Cao A, Garg N, Dhiman M, Pyles RB, Arulanandam B, Miller AL et al. Immunomodulatory and antibacterial effects of cystatin 9 against *Francisella tularensis*. *Mol Med* 2013;**19**:263–275.
- Engelberg Y, Landau M. The human LL-37(17-29) antimicrobial peptide reveals a functional supramolecular structure. *Nat Commun* 2020;**11**:3894.
- Fowler DM, Koulov AV, Balch WE, Kelly JW. Functional amyloid—from bacteria to humans. *Trends Biochem Sci* 2007;**32**:217–224.
- Gu L, Guo ZF. Lipid membranes induce structural conversion from amyloid oligomers to fibrils. *Biochem Biophys Res Commun* 2021;**557**:122–126.
- Hall SH, Hamil KG, French FS. Host defense proteins of the male reproductive tract. *J Androl* 2002;**23**:585–597.
- Hall SH, Yenugu S, Radhakrishnan Y, Avellar MCW, Petrusz P, French FS. Characterization and functions of beta defensins in the epididymis. *Asian J Androl* 2007;**9**:453–462.
- Hamil KG, Liu Q, Sivashanmugam P, Yenugu S, Soundararajan R, Grossman G, Richardson RT, Zhang YL, O'Rand MG, Petrusz P et al. Cystatin 11: a new member of the cystatin type 2 family. *Endocrinology* 2002;**143**:2787–2796.
- Hewetson A, Do HQ, Myers C, Muthusubramanian A, Sutton RB, Wylie BJ, Cornwall GA. Functional amyloids in reproduction. *Biomolecules* 2017;**7**:46.
- Hewetson A, Khan NH, Dominguez MJ, Do HQ, Kusko RE, Borcik CG, Rigden DJ, Keegan RM, Sutton RB, Latham MP et al. Maturation of the functional mouse CRES amyloid from globular form. *Proc Natl Acad Sci U S A* 2020;**117**:16363–16372.
- Hjelm A, Soderstrom B, Vikstrom D, Jong WSP, Luirink J, de Gier JW. Autotransporter-based antigen display in bacterial ghosts. *Appl Environ Microbiol* 2015;**81**:726–735.
- Holloway AJ, Yu J, Arulanandam BP, Hoskinson SM, Eaves-Pyles T. Cystatins 9 and C as a novel immunotherapy treatment that protects against multidrug-resistant New Delhi metallo-beta-lactamase-1-producing *Klebsiella pneumoniae*. *Antimicrob Agents Chemother* 2018;**62**:e01900–17.
- Huang P, Li WS, Yang ZF, Zhang N, Xu YX, Bao JY, Jiang DK, Dong XP. LYZL6, an acidic, bacteriolytic, human sperm-related protein, plays a role in fertilization. *PLoS One* 2017;**12**:e0171452.
- Jenssen H, Hancock REW. Antimicrobial properties of lactoferrin. *Biochimie* 2009;**91**:19–29.
- Jin YZ, Bannai S, Dacheux F, Dacheux JL, Okamura N. Direct evidence for the secretion of lactoferrin and its binding to sperm in the porcine epididymis. *Mol Reprod Dev* 1997;**47**:490–496.

- Kagan BL, Jang H, Capone R, Arce FT, Ramachandran S, Lal R, Nussinov R. Antimicrobial properties of amyloid peptides. *Mol Pharm* 2012;**9**:708–717.
- Kai-Larsen Y, Luthje P, Chromek M, Peters V, Wang XD, Holm A, Kadas L, Hedlund KO, Johansson J, Chapman MR et al. Uropathogenic *Escherichia coli* modulates immune responses and its curli fimbriae interact with the antimicrobial peptide LL-37. *PLoS Pathog* 2010;**6**:e1001010.
- Lang TL, Dechant M, Sanchez V, Wistuba J, Boiani M, Pilatz A, Stammler A, Middendorff R, Schuler G, Bhushan S et al. Structural and functional integrity of spermatozoa is compromised as a consequence of acute uropathogenic *E. coli*-associated epididymitis. *Biol Reprod* 2013;**89**:59.
- Langemann T, Koller V, Muhammad A, Pavol K, Ulrike B, Lubitz W. The bacterial ghost platform system: production and applications. *Bioeng Bugs* 2010;**1**:326–336.
- Malm J, Sørensen O, Persson T, Frohm-Nilsson M, Johansson B, Bjartell A, Lilja H, Ståhle-Bäckdahl M, Borregaard N, Egesten A. The human cationic antimicrobial protein (hCAP-18) is expressed in the epithelium of human epididymis, is present in seminal plasma at high concentrations, and is attached to spermatozoa. *Infect Immun* 2000;**68**:4297–4302.
- Michel V, Duan Y, Stoschek E, Bhushan S, Middendorff R, Young JM, Loveland KL, De Kretser DM, Hedger MP, Meinhardt A. Uropathogenic *Escherichia coli* causes fibrotic remodelling of the epididymis. *J Pathol* 2016;**240**:15–24.
- Michel V, Pilatz A, Hedger MP, Meinhardt A. Epididymitis: revelations at the convergence of clinical and basic sciences. *Asian J Androl* 2015;**17**:756–763.
- Nilsson MR, Dobson CM. In vitro characterization of lactoferrin aggregation and amyloid formation. *Biochemistry* 2003;**42**:375–382.
- Pham CLL, Kwan AH, Sunde M. Functional amyloid: widespread in Nature, diverse in purpose. *Essays Biochem* 2014;**56**:207–219.
- Pilatz A, Hossain H, Kaiser R, Mankertz A, Schuttler CG, Domann E, Schuppe HC, Chakraborty T, Weidner W, Wagenlehner F. Acute epididymitis revisited: impact of molecular diagnostics on etiology and contemporary guideline recommendations. *Eur Urol* 2015;**68**:428–435.
- Pleuger C, Silva EJR, Pilatz A, Bhushan S, Meinhardt A. Differential immune response to infection and acute inflammation along the epididymis. *Front Immunol* 2020;**11**:599594.
- Schwartz K, Boles BR. Microbial amyloids—functions and interactions within the host. *Curr Opin Microbiol* 2013;**16**:93–99.
- Silva EJR, Patrao M, Tsuruta JK, O’Rand MG, Avellar MCW. Epididymal protease inhibitor (EPPIN) is differentially expressed in the male rat reproductive tract and immunolocalized in maturing spermatozoa. *Mol Reprod Dev* 2012;**79**:832–842.
- Soria MA, Cervantes SA, Bajakian TH, Siemer AB. The functional amyloid Orb2A binds to lipid membranes. *Biophys J* 2017;**113**:37–47.
- Tung KSK, Harakal J, Qiao H, Rival C, Li JCH, Paul AGA, Wheeler K, Pramoonjago P, Grafer CM, Sun W et al. Egress of sperm auto-antigen from seminiferous tubules maintains systemic tolerance. *J Clin Invest* 2017;**127**:1046–1060.
- Wang JR, Li Y, Wang XM, Chen W, Sun HB, Wang JF. Lipopolysaccharide induces amyloid formation of antimicrobial peptide HAL-2. *Biochim Biophys Acta* 2014;**1838**:2910–2918.
- Wang L, Yuan Q, Chen SH, Cai H, Lu MG, Liu Y, Xu C. Antimicrobial activity and molecular mechanism of the CRES protein. *Plos One* 2012;**7**:e48368.
- Wassler M, Syntin P, Sutton-Walsh HG, Hsia N, Hardy DM, Cornwall GA. Identification and characterization of cystatin-related epididymal spermatogenic protein in human spermatozoa: Localization in the equatorial segment. *Biol Reprod* 2002;**67**:795–803.
- Wei J, Li S-J, Shi H, Wang H-Y, Rong C-T, Zhu P, Jin S-H, Liu J, Li J-Y. Characterisation of Lyzls in mice and antibacterial properties of human LYZL6. *Asian J Androl* 2013;**15**:824–830.
- Wheeler K, Tardif S, Rival C, Luu B, Bui E, del Rio R, Teuscher C, Sparwasser T, Hardy D, Tung KSK. Regulatory T cells control tolerogenic versus autoimmune response to sperm in vasectomy. *Proc Natl Acad Sci U S A* 2011;**108**:7511–7516.
- Whelly S, Johnson S, Powell J, Borchardt C, Hastert MC, Cornwall GA. Nonpathological extracellular amyloid is present during normal epididymal sperm maturation. *PLoS One* 2012;**7**:e36394.
- Whelly S, Muthusubramanian A, Powell J, Johnson S, Hastert MC, Cornwall GA. Cystatin-related epididymal spermatogenic subgroup members are part of an amyloid matrix and associated with extracellular vesicles in the mouse epididymal lumen. *Mol Hum Reprod* 2016;**22**:729–744.
- Witte A, Lubitz W. Biochemical characterization of phi X174-protein-E-mediated lysis of *Escherichia coli*. *Eur J Biochem* 1989;**180**:393–398.
- Witte A, Wanner G, Sulzner M, Lubitz W. Dynamics of phi X174 protein E-mediated lysis of *Escherichia coli*. *Arch Microbiol* 1992;**157**.
- Yenugu S, Hamil KG, Birse CE, Ruben SM, French FS, Hall SH. Antibacterial properties of the sperm-binding proteins and peptides of human epididymis 2 (HE2) family; salt sensitivity, structural dependence and their interaction with outer and cytoplasmic membranes of *Escherichia coli*. *Biochem J* 2003;**372**:473–483.
- Yenugu S, Narmadha G. The human male reproductive tract antimicrobial peptides of the HE2 family exhibit potent synergy with standard antibiotics. *J Pept Sci* 2010;**16**:337–341.
- Yenugu S, Richardson RT, Sivashanmugam P, Wang ZJ, O’Rand MG, French FS, Hall SH. Antimicrobial activity of human EPPIN, an androgen-regulated, sperm-bound protein with a whey acidic protein motif. *Biol Reprod* 2004;**71**:1484–1490.
- Zhou CX, Zhang Y-L, Xiao L, Zheng M, Leung KM, Chan MY, Lo PS, Tsang LL, Wong HY, Ho LS et al. An epididymis-specific beta-defensin is important for the initiation of sperm maturation. *Nat Cell Biol* 2004;**6**:458–464.